

Phase Separation and Domain Formation in Multi-Component Membranes: Finsler Geometry Modeling and Monte Carlo Simulations

Satoshi Usui¹ and Hiroshi Koibuchi²

¹Advanced course of Mechanical Engineering, National Institute of Technology, Ibaraki College, Japan

²Department of Mechanical and Systems, National Institute of Technology, Ibaraki College, Japan

Abstract. In this paper, we study a surface model for membranes of three components such as DPPC, DOPC, and Cholesterol. This membrane is experimentally well known to undergo the phase separation and to form the domain structure such as the liquid ordered (L_o) phase and the liquid disordered phase (L_d). It is also well known that this multicomponent membrane has a lot of domain pattern transitions between the circular domains and the striped domain etc. Using the new surface model constructed on the basis of Finsler geometry, we study why those morphological changes appear on the spherical vesicles. In our model, we introduce a new variable $\sigma (\in Z_2)$ to represent the domains L_o and L_d , and using the value of σ we define a metric function on the surface. As a consequence, the origin of the line tension energy, which has been used to explain the domain pattern transition in the multicomponent membranes, is naturally understood in our model.

1 Introduction

Artificial membranes such as vesicles are used to study the mechanism of biological cell membranes [1]. The vesicles, which are composed of saturated phospholipids, unsaturated phospholipids, and cholesterol, undergo a phase separation and a domain pattern transition [2]. After the phase separation, two types of domains appear: one is the liquid ordered (L_o) phase, which is rich in the saturated phospholipids and cholesterol, and the other is the liquid disordered (L_d) phase, which is rich in the unsaturated phospholipids.

These two domains cause the domain pattern transition, which accompanies the shape deformation [2]. For example, the oblate shape membranes with two Circular L_o Domains (2CD) such as **Fig.1** (a), and the prolate shape membranes with one Striped L_o Domain (1SD) such as **Fig.1** (b) are well known. It is also well known that the L_o phase forms many round domains, and this domain structure is very similar to the so called lipid raft.

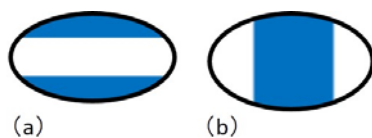


Figure 1. General form of (a) 1SD, and (b) 2CD. The blue (white) region corresponds to L_o (L_d) phase.

However, the mechanism of shape deformation is still unclear, although a lot of theoretical studies have been conducted. For example, the mechanism of shape deformation to 2CD and 1SD can be explained by using the models with the line tension on the boundary between L_o and L_d phases [3, 4]. However, the origin of the line tension is unknown. The problem that should be asked is the microscopic origin of the line tension.

The purpose of this study is to find the origin of the line tension and clarify the mechanism of shape deformation, which is produced by the phase separation. For this purpose, we define a Finsler geometry surface model [5] by extending the conventional Helfrich-Polyakov model for membranes [6, 7]. In the new model, we introduce a new degree of freedom $\sigma (\in Z_2)$, which corresponds to the two phases L_o and L_d . The interaction between this σ and the membrane shape is naturally introduced by a Finsler metric, which is defined by using the value of σ .

2 Model

2.1 Continuous model

The Hamiltonian (=energy function) of the continuous mode is defined by a mapping \mathbf{r} from a two-dimensional surface M to the three-dimensional Euclidean space \mathbf{R}^3 . The continuous description of the Hamiltonian is as follows:

$$\begin{aligned}
S &= \lambda S_0 + S_1 + \kappa S_2, \\
S_0 &= \frac{1}{2} \int \sqrt{g} dx^2 g^{ab} \frac{\partial \sigma}{\partial x_a} \cdot \frac{\partial \sigma}{\partial x_b}, \\
S_1 &= \int \sqrt{g} dx^2 g^{ab} \frac{\partial \mathbf{r}}{\partial x_a} \cdot \frac{\partial \mathbf{r}}{\partial x_b}, \\
S_2 &= \frac{1}{2} \int \sqrt{g} dx^2 g^{ab} \frac{\partial \mathbf{n}}{\partial x_a} \cdot \frac{\partial \mathbf{n}}{\partial x_b}.
\end{aligned} \tag{1}$$

The metric tensor is given by

$$g_{ab} = \begin{pmatrix} \rho^{-1} & 0 \\ 0 & \rho \end{pmatrix}, \quad \rho > 0, \tag{2}$$

where ρ is a function on the surface. The inverse metric and the determinant are $g^{ab} = (g_{ab})^{-1}$, $g = \det(g_{ab})$.

The metric g_{ab} in Eq.(2) comes from the most general metric such as $g_{ab} = \begin{pmatrix} E & F \\ F & G \end{pmatrix}$, with the conditions $E > 0, G > 0, EG - F^2 > 0$.

2.2 Discrete model

The discrete Hamiltonian is obtained by a discretization of the continuous Hamiltonian in (1) on the triangulated lattices such as **Fig.2**. The discrete model is considered as a Finsler geometry model [5]. We should note that the Finsler function $L = \sqrt{\sum_{\Delta} L_{\Delta}^2}$ is given by this metric such that $L_{\Delta}^2 = \rho^{-1} y_1^2 + \rho y_2^2 = \sum_{\Delta} g_{ab} y_a y_b$, where x_a ($a = 1, 2$) is a local coordinate along the bond, and $y_a = \dot{x}_a$ is a tangential vector along the local coordinate or bond.

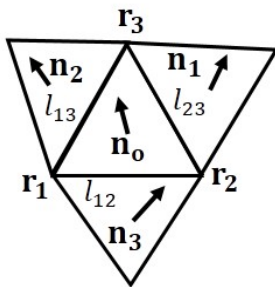


Figure 2. Triangles for the discretization, the vertex positions $\mathbf{r}_1, \mathbf{r}_2, \mathbf{r}_3$, the unit normal vectors $\mathbf{n}_0, \mathbf{n}_1, \mathbf{n}_2, \mathbf{n}_3$.

Assuming that the vertex position \mathbf{r}_1 is the local coordinate origin, we replace the symbols in (1) as follows :

$$\begin{aligned}
\int \sqrt{g} dx^2 &\rightarrow \sum_{\Delta}, \\
\frac{\partial \mathbf{r}}{\partial x_1} &\rightarrow \mathbf{r}_2 - \mathbf{r}_1 = l_{12}, \quad \frac{\partial \mathbf{r}}{\partial x_1} \rightarrow \mathbf{r}_3 - \mathbf{r}_1 = l_{13}, \\
\frac{\partial \mathbf{n}}{\partial x_1} &\rightarrow \mathbf{n}_0 - \mathbf{n}_2, \quad \frac{\partial \mathbf{n}}{\partial x_1} \rightarrow \mathbf{n}_0 - \mathbf{n}_3.
\end{aligned} \tag{3}$$

From (1) and (3), we get

$$\begin{aligned}
S_1 &= \sum_{\Delta} \left(\rho l_{12}^2 + \frac{1}{\rho} l_{13}^2 \right), \\
S_2 &= \sum_{\Delta} \left(\rho (1 - \mathbf{n}_0 \cdot \mathbf{n}_2) + \frac{1}{\rho} (1 - \mathbf{n}_0 \cdot \mathbf{n}_3) \right)
\end{aligned} \tag{4}$$

Not only \mathbf{r}_1 , but also \mathbf{r}_2 and \mathbf{r}_3 can be chosen as the local coordinate origin. Therefore, by the cyclic permutations $1 \rightarrow 2, 2 \rightarrow 3, 3 \rightarrow 1$ for the expressions in Eq. (4) and with the factor 1/3, we have

$$\begin{aligned}
S_1 &= \frac{1}{3} \sum_{\Delta} \left(\rho + \frac{1}{\rho} \right) (l_{12}^2 + l_{23}^2 + l_{31}^2), \\
S_2 &= \frac{1}{3} \sum_{\Delta} \left(\rho + \frac{1}{\rho} \right) \\
&\quad (1 - \mathbf{n}_0 \cdot \mathbf{n}_1 + 1 - \mathbf{n}_0 \cdot \mathbf{n}_2 + 1 - \mathbf{n}_0 \cdot \mathbf{n}_3).
\end{aligned} \tag{5}$$

In the expressions of Eq. (5), we assume that the function ρ is independent of the choice of the local coordinate, where ρ is originally dependent on the local coordinate.

By replacing the sum over triangles with the sum over bonds, and replacing the numerical factor 2/3 with 1/4, we get

$$\begin{aligned}
S_1 &= \frac{1}{4} \sum_{ij} \left(\rho_i + \frac{1}{\rho_i} + \rho_j + \frac{1}{\rho_j} \right) l_{ij}^2, \\
S_2 &= \frac{1}{4} \sum_{ij} \left(\rho_i + \frac{1}{\rho_i} + \rho_j + \frac{1}{\rho_j} \right) (1 - \mathbf{n}_i \cdot \mathbf{n}_j).
\end{aligned} \tag{6}$$

The triangles are separated into two groups L_o and L_d , which are labeled by σ (see **Fig.3**). (Don't confuse the letters for domains and the one for Finsler function.)

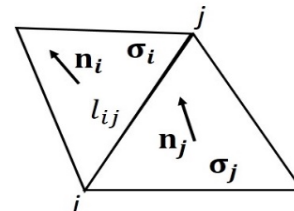


Figure 3. Geometrical quantities on the two neighboring triangles of the bond ij (on a triangulated spherical surface).

The discrete Hamiltonian can be written as

$$\begin{aligned}
S &= \lambda S_0 + S_1 + \kappa S_2, \\
S_0 &= \sum_{(i,j)} (1 - \sigma_i \cdot \sigma_j), \\
S_1 &= \sum_{(i,j)} \gamma_{ij} l_{ij}^2, \quad S_2 = \sum_{(i,j)} \kappa_{ij} (1 - \mathbf{n}_i \cdot \mathbf{n}_j), \\
\gamma_{ij} &= \kappa_{ij} = \frac{c_i + c_j}{4}, \quad c_i = \rho_i + \frac{1}{\rho_i}, \\
\rho(\Delta) &= \begin{cases} c & (\Delta \in L_o) \\ 1 & (\Delta \in L_d) \end{cases}, \\
\sigma(\Delta) &= \begin{cases} 1 & (\Delta \in L_o) \\ -1 & (\Delta \in L_d) \end{cases}
\end{aligned} \tag{7}$$

where S_0 is the aggregation energy, and σ (Fig.3) is the function on the triangle such that $\sigma = 1$ ($\sigma = -1$) if the triangle Δ is included in L_o (L_d). This S_0 corresponds to the line tension on the boundary between L_o and L_d , because the value of S_0 is proportional to the length of the boundary. S_1 is the Gaussian bond potential, where the symbol l_{ij} denotes the length of the bond ij (Fig.2). S_2 is the bending energy, where the symbol \mathbf{n}_i denotes the unit normal vector of the triangle i (Fig.3). The quantities γ_{ij} and κ_{ij} are respectively called effective surface tension and effective bending rigidity. Both quantities are defined by using a function ρ on the triangle, which is defined such that $\rho = c$ ($\rho = 1$) if the triangle Δ is included in L_o (L_d).

The effective surface tension γ_{ij} is defined by ρ of two neighboring triangles, as mentioned above. For this reason γ_{ij} has three different values such that $\gamma_{ij} = (c + 1/c)/2$ for L_o and L_o (Fig.4(a)), $\gamma_{ij} = (2 + c + 1/c)/4$ for L_o and L_d (Fig.4(b)), and $\gamma_{ij} = 1$ for L_d and L_d (Fig.4(c)). For κ_{ij} , we also have three different values, which are exactly the same as those for γ_{ij} . We should note that these γ_{ij} and κ_{ij} depend on the position and the direction on the surface, because these are defined on the bonds by using ρ 's on the two neighboring triangles. Moreover, γ_{ij} and κ_{ij} are symmetric under the exchange of i and j ($\gamma_{ij} = \gamma_{ji}$, $\kappa_{ij} = \kappa_{ji}$).

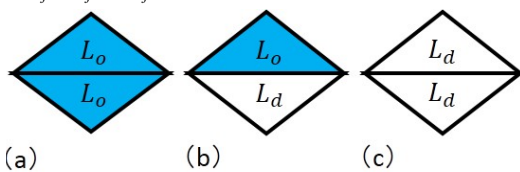


Figure 4. Three types of combinations of the triangles (a) L_o and L_o , (b) L_o and L_d , (c) L_d and L_d .

3 Simulation technique

We use the Monte Carlo (MC) technique for the membrane simulation [8, 9]. In this MC technique, the vertex position \mathbf{r} is randomly moved to $\mathbf{r}' = \mathbf{r} + \delta\mathbf{r}$ (Fig.5) with the probability

$$\text{Min}[1, \exp(-\delta S)], \tag{8}$$

where $\delta S = S_{\text{new}} - S_{\text{old}}$. This implies that \mathbf{r} is updated to \mathbf{r}' with the probability $1 - \exp(-\delta S)$ if $\delta S < 0$ ($\delta S > 0$).

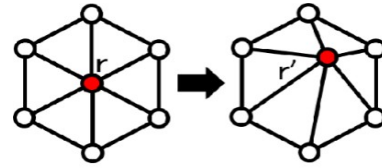


Figure 5. MC update of the vertex position \mathbf{r} to $\mathbf{r}' = \mathbf{r} + \delta\mathbf{r}$

In this study, the lattice structure is changed by bond flip technique such as in Fig.6 This bond flip makes the vertices diffuse freely over the surface, and hence the surface becomes a fluid surface. After the bond flip, σ_i and σ_j , which are the functions on the triangle i and j , change to σ'_i and σ'_j , which are the functions on the triangle i' and j' . In this process, we assume that the total number of triangles in L_o (and L_d) phase remains unchanged such that $\sigma'_i = \sigma'_j$ if $\sigma_i = \sigma_j$, and $\sigma'_i \neq \sigma'_j$ if $\sigma_i \neq \sigma_j$. In the latter case, the new values are randomly chosen from $\{1, -1\}$ (Fig.7). Thus, the free diffusion of vertices due to the dynamical triangulation forms the domain boundary between L_o and L_d on the surface. This bond flip process is essential for the domain formation.

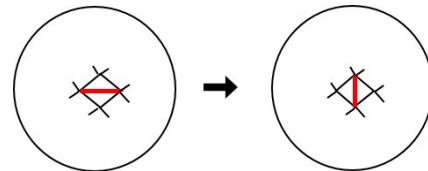


Figure 6. A bond flip as a MC process, which makes the surface fluid.

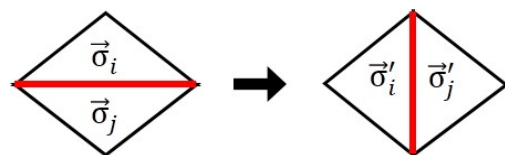


Figure 7. The variable σ is changed by the bond flips over the surface.

4 Simulation results

In this study, we perform the simulations for two types of models: model 1 and model 2.

Model 1 is defined by $\gamma_{ij} = 1$, where the Finsler metric is introduced only in S_2 . S_1 in model 1 is just the same as that of the ordinary model. In model 2, the Finsler metric is introduced in both S_1 and S_2 .

4.1 Model 1

The parameters used in the simulations for model 1 are shown in **Tables 1, 2**. The input parameters by hand are λ , which is the coefficient of S_0 in (4), $\phi_o (= N_{L_o} / N_T)$ (N_{L_o}, N_T are the total number of L_o triangles and the total number of triangles), which is the area fraction of L_o phase, the bending rigidity \mathcal{K} . These are listed in **Tables 1**. \mathcal{C} is the parameter for the function ρ in (4). The value of \mathcal{C} here, we assumed is $c = 0.05$.

Table 1. The parameters for the simulations for model 1. λ , ϕ_o , and \mathcal{K} are fixed by hand as the inputs.

	λ	ϕ_o	\mathcal{K}
(a)	0.25	0.7	7
(b)	0.2	0.5	7
(c)	0.08	0.4	7
(d)	3.0	0.65	7

The parameters \mathcal{K}_{ij} is automatically determined according to the combination of the two neighboring triangles as listed in **Tables 2**.

Table 2. The parameters for the simulations for model 1. The bending rigidity \mathcal{K}_{ij} are automatically fixed.

	$\mathcal{K}_{ij}(L_o, L_o)$	$\mathcal{K}_{ij}(L_o, L_d)$	$\mathcal{K}_{ij}(L_d, L_d)$
(a)	10	5.5	1
(b)	10	5.5	1
(c)	10	5.5	1
(d)	10	5.5	1

Snapshots of the surface of the lattice size $N = 5762$ are shown in **Fig.8**. The L_o domain is 10 times more rigid than the L_d domain, because $\mathcal{K}_{ij}(L_o, L_o) = 10$ and $\mathcal{K}_{ij}(L_d, L_d) = 1$. At the domain boundary, the surface stiffness is fixed to the intermediate value of these two such that $\mathcal{K}_{ij}(L_o, L_d) = 5.5$. We see from **Fig.8(a)** that 1SD appears if λ and ϕ_o are large, also from **Fig.8(b)** that 2CD appears if λ and ϕ_o are small. Therefore, the membrane shape changes 1SD to 2CD, if λ and ϕ_o

are reduced. We also find from **Fig.8(c)** that a random pattern appears if λ is very small, where the domains are not separated. Moreover, we find from **Fig.8(d)** that the budding appears. The budding is a phase with the domains which grow inside or outside the surface.

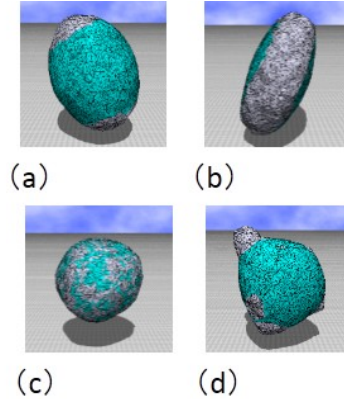


Figure 8. Snapshots of the surfaces corresponding to the domains (a) 1SD, (b) 2CD, (c) random, (d) budding, which are obtained from the simulations for model 1

4.2 Model 2

The parameters used in the simulations for model 1 are shown in **Tables 3, 4**. The parameters γ_{ij} and \mathcal{K}_{ij} are automatically determined from the combination of the neighboring triangles and the value of c . This is the same as that of model 1 in the previous subsection. Here, we assume $c = 0.084$ and $c = 0.05$ for (a), (b) and (c), (d), respectively.

Table 3. The parameters for the simulations for model 2. λ , ϕ_o , and \mathcal{K} are fixed by hand as the inputs.

	λ	ϕ_o	\mathcal{K}
(a)	0.5	0.9	10
(b)	0.2	0.7	10
(c)	1.5	0.65	7
(d)	1.5	0.8	7

Table 4. The parameters for the simulations of model 2. the bending rigidity \mathcal{K}_{ij} , and the surface tension γ_{ij} are automatically fixed.

	$\mathcal{K}_{ij}(L_o, L_o)$, $\gamma_{ij}(L_o, L_o)$	$\mathcal{K}_{ij}(L_o, L_d)$, $\gamma_{ij}(L_o, L_d)$	$\mathcal{K}_{ij}(L_d, L_d)$, $\gamma_{ij}(L_d, L_d)$
(a)	6	3.5	1
(b)	6	3.5	1
(c)	10	5.5	1
(d)	10	5.5	1

Snapshots of the surface of the lattice size $N = 5762$ are shown in **Fig.9**.

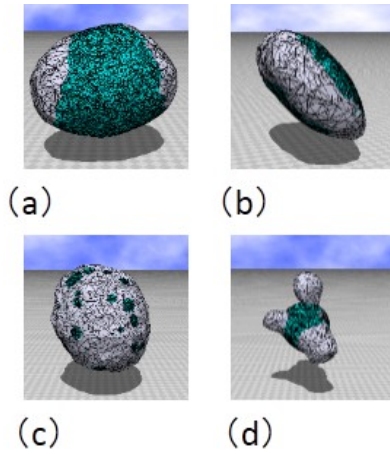


Figure 9. Snapshots of the surfaces corresponding to the domains (a) 1SD, (b) 2CD, (c) raft, (d) budding, which are obtained from the simulations for model 2.

In this simulations, we find that the surface shape changes 1SD to 2CD, if λ and κ are reduced, just as in the cases of model 1. Moreover, we find from **Fig.9(c)** that the raft appears. The raft is a phase of the multi circular domains. The budding also appears, if λ is very large. These raft and budding can be seen in the real multi-component membranes.

5 Conclusions

In this paper, we study a coarse grained Finsler geometric surface model for three components membrane. The purpose is to understand the origin of the line tension on the boundary between L_o and L_d phases in those membranes. We have performed Monte Carlo simulations on the dynamically triangulated spherical surfaces.

The results are summarised as follows.

1. The domain 1SD (2CD) appears if both λ and ϕ_o are large (small).
2. The domain structure changes from 1SD to 2CD (from 2CD to 1SD) if both λ and ϕ_o are decreased (increased).
3. The bending rigidity for L_o domain ($\kappa_{ij}(L_o, L_o)$) is relatively large, therefore L_o domain is smoother than the L_d domain.

These results obtained in both models 1 and 2 are consistent with the experimental results. Recalling that the aggregation energy S_0 is proportional to the length of the boundary between L_o and L_d phases, we find that the interaction of σ with the surface is considered as the origin of the line tension on the boundary. This interaction between σ and the surface is introduced by the Finsler metric, and therefore, the origin of the line tension energy is understood in the context of Finsler geometry modeling of membranes.

In the model of this paper, we assume that the function ρ used in the Finsler metric is independent of

the local coordinate on the triangle. For this reason, the effective surface tension and bending rigidity become symmetric $\gamma_{ij} = \gamma_{ji}$, $\kappa_{ij} = \kappa_{ji}$. Because of this property, the Hamiltonian of the surface is identical with that of the inverted surface. This implies that the model introduced in this paper is able to describe the area difference and the spontaneous curvature, both of which separates the spherical membrane from the inverted membranes, if the assumption for ρ is neglected. Therefore, it is interesting to study the origin of spontaneous curvature and area difference in bilayer membranes in the context of Finsler geometry modeling. The problem that will be asked is the microscopic origin of spontaneous curvature and area difference in bilayer membranes. This will be the future study.

References

1. D. Nelson, in *Statistical Mechanics of Membranes and Surfaces, Second Edition*, edited by D. Nelson, T. Piran, and S. Weinberg, (World Scientific, Singapore, 2004) p.1.
2. M. Yanagisawa, M. Imai, and T. Taniguchi, *Physical Review Letters*, **100**, 148102, (2008).
3. E. Gutleiderer, T. Gruhn, and R. Lipowsky, **5**, pp. 3303-3311, (2009).
4. M. Yanagisawa, M. Imai, and T. Taniguchi, *Physical Review E* **82**, 051928, (2010).
5. H. Koibuchi and H. Sekino, *Physica A* **393**, pp. 37-50, (2014).
6. W. Helfrich, *Z. Naturforsch*, 28c (1973) 693.
7. A.M. Polyakov, *Nucl. Phys. B* **268** (1986) 406.
8. N. Metropolis, A. W. Rosenbluth, M. N. Rosenbluth and A. H. Teller, *J. Chem. Phys.* **21**, 1087 (1953).
9. D.P. Landau, *Phys. Rev. B* **13**, 2997 (1976).